



# Long-lasting activity of $\text{Fe}^0$ -C internal microelectrolysis-Fenton system assisted by Fe@C-montmorillonites nanocomposites

Hongyun Niu<sup>a,\*</sup>, Dongwei He<sup>a,b</sup>, Yongliang Yang<sup>a,c</sup>, Hongzhou Lv<sup>a,d,e</sup>, Yaqi Cai<sup>a,b,c</sup>, Yong Liang<sup>b</sup>



<sup>a</sup> State Key Laboratory of Environmental Chemistry and Ecotoxicology, Research Center for Eco-Environmental Sciences, Chinese Academy of Sciences, Beijing, 100085, China

<sup>b</sup> Institute of Environment and Health, Jianghan University, Wuhan, 430056, China

<sup>c</sup> University of Chinese Academy of Sciences, Beijing, 100049, China

<sup>d</sup> College of Environment, Hohai University, Nanjing, 210098, China

<sup>e</sup> State Key Laboratory of Environmental Criteria and Risk Assessment, Chinese Research Academy of Environmental Sciences, Beijing, 100012, China

## ARTICLE INFO

### Keywords:

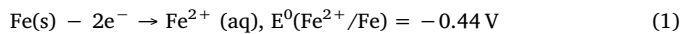
Internal microelectrolysis-Fenton  
Montmorillonites  
Fenton reaction  
Phenol  
Methyl orange

## ABSTRACT

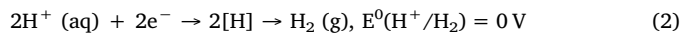
Core/shell type  $\text{Fe}^0$ @carbon (Fe@C) nanocomposites inserted in the interlayer space of montmorillonites (MMT) is prepared by one-step pyrolysis of Fe-metal organic frameworks and MMT. Fe@C-MMT serves as Fenton-like catalyst to degrade organic pollutants based on internal microelectrolysis (IME)-Fenton reactions. The MMT coat accelerates galvanic corrosion of  $\text{Fe}^0$  to facilitate in-situ generation of  $\text{Fe}^{2+}$  and achieves self-regulation of solution pH. Strengthened elimination of phenol and methyl orange with high mineralization efficiency (80%) at initial pH 3–6.5 was achieved in Fe@C-MMT- $\text{H}_2\text{O}_2$  system compared to Fe@C-, ZVI-, and commercial Fe-C- $\text{H}_2\text{O}_2$  systems. The MMT coat retards contact of  $\text{Fe}^0$  and Fe(II) species on Fe@C-MMT surface with  $\text{H}_2\text{O}_2$ , leading to rate-controlling consumption of  $\text{H}_2\text{O}_2$  to keep the long-lasting efficiency of the IME-Fenton system. Fe@C-MMT suspension with 10 mM of  $\text{H}_2\text{O}_2$  can continuously degrade organic pollutants within 40 h. Fe@C-MMT can be recycled for five times and shows good resistance to oxygen and acid corrosion.

## 1. Introduction

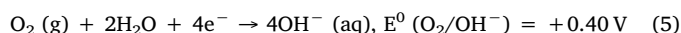
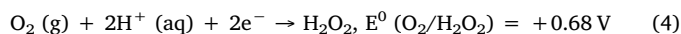
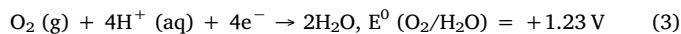
Over the decades, iron carbon (Fe-C) internal microelectrolysis (IME) has been widely used to remove bio-refractory components from industrial wastewater due to extensive adaptability to wastewater with various compositions [1–7]. IME process works based on the electrochemical reactions of microscopic galvanic cells between the electrode materials (iron and carbon) in the acidic solution [1]. The electrode reactions can be represented as follows (Eqs. (1)–(5)):



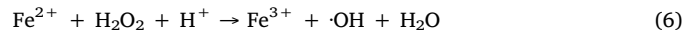
Carbon cathode (reduction):



In the presence of oxygen:



Products released from galvanic cell reaction, including atomic hydrogen and Fe(II), have high activities and are easy to react with contaminants [2–6]. Under aerated conditions, the dissolved oxygen can compete with  $\text{H}^+$  as an electron acceptor to produce  $\text{H}_2\text{O}_2$  (Eq. (4)). The in-situ generated  $\text{H}_2\text{O}_2$  subsequently combines with ferrous ions, released by galvanic corrosion of iron scraps, to yield highly reactive hydroxyl radicals ( $\cdot\text{OH}$ ) (Eq. (6)) to non-selectively degrade organic pollutants [1,3].



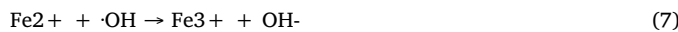
However, the oxidation ability of reactive substances produced in IME reactions and  $\text{H}_2\text{O}_2$  in-situ generation efficiency are relatively low, leading to low degradation efficiency of recalcitrant organic contaminants by the Fe-C IME technology [1].

Combination of Fe-C IME with Fenton reaction improves the wastewater treatment efficiency greatly [8–11]. The  $\text{Fe}^{2+}$  species produced in  $\text{Fe}^0$  anode catalyzes the decomposition of  $\text{H}_2\text{O}_2$ . The continuous release of  $\text{Fe}^{2+}$  via galvanic corrosion avoids invalid decomposition of  $\text{H}_2\text{O}_2$  to form  $\text{O}_2$  as a reaction product in addition to superoxide radical ( $\text{O}_2\cdot-$ ). But the selective decomposition of  $\text{H}_2\text{O}_2$  to  $\cdot\text{OH}$  radicals does

\* Corresponding author.

E-mail address: [hy niu@rcees.ac.cn](mailto:hy niu@rcees.ac.cn) (H. Niu).

not necessarily mean high utilization efficiency of  $\text{H}_2\text{O}_2$  [12]. The fast and fiercely produced high concentration of  $\cdot\text{OH}$  radicals in a short time can be consumed not only by organic pollutants but also by  $\text{H}_2\text{O}_2$ ,  $\text{Fe}^{2+}$ , and ROS (Eqs. (7)–(9)) [13–16], which leads to incomplete mineralization of organic pollutants and decreases the utilization efficiency of  $\text{H}_2\text{O}_2$ .



Therefore, rate-limiting and selective decomposition of  $\text{H}_2\text{O}_2$  toward  $\cdot\text{OH}$  radicals in Fenton reaction is essential to ensure continuous production of  $\cdot\text{OH}$  radicals and guarantee the long-lasting efficiency of IME-Fenton system. The nanocrystalline iron or iron oxide-based heterogeneous catalysts exhibit variable efficiencies in the  $\text{H}_2\text{O}_2$  decomposition, with rate constants ranging from  $10^{-5}$  to  $10^{-2} \text{ min}^{-1}$ . The particles' size, crystallinity, porosity, and surface area of these Fe-based catalysts determine the variability in the decomposition rate of  $\text{H}_2\text{O}_2$  [17,18]. Thereby, continuous formation of hydroxyl free radicals through rate-limiting decomposition of  $\text{H}_2\text{O}_2$  could be achieved by synthesis of iron nanocomposites with suitable crystalline and surface properties.

Montmorillonites (MMT) are natural layered clays whose structure is formed by  $\text{AlO}_6$  octahedra sandwiched by  $\text{SiO}_4$  tetrahedra. MMT have been utilized as good supporting materials for metal or metal oxides catalysts to prevent their aggregation, but also as adsorbents and heterogeneous Fenton catalysts for water purification [19–28]. MMT is always negatively charged in a wider pH range (2–11) in water [19,29], which is favorable for the adsorption of  $\text{H}_2\text{O}_2$  onto its surface and accordingly beneficial for the rate-controlling  $\text{H}_2\text{O}_2$  decomposition in reaction [27]. The negative surface is helpful for the formation of a proton concentrated layer over MMT surface, so that the selectivity of  $\text{H}_2\text{O}_2$  decomposition toward  $\cdot\text{OH}$  radicals would be enhanced [27,29]. It is can be anticipated that the introduction of MMT in  $\text{Fe}^{0-}\text{C}$  can improve the removal of pollutants via adsorption and enhance the utilization efficiency of  $\text{H}_2\text{O}_2$ . In the present study, we applied montmorillonite KSF, which is an acid modified montmorillonite and contains a higher content of iron than ordinary MMT [21], as the support of core/shell structured  $\text{Fe}@\text{C}$  nanocomposites. With the assistant of MMT, the catalytic performance of  $\text{Fe}@\text{C}$ -MMT in IME-Fenton system clearly improved and the utilization efficiency of  $\text{H}_2\text{O}_2$  enhanced greatly compared to  $\text{Fe}@\text{C}$  and ZVI.

## 2. Materials and methods

### 2.1. Reagents and materials

Titanium sulphate, 1,10-phenanthroline, tetramethylammonium hydroxide (v/v 25%), 1,4-benzenedicarboxylic acid ( $\text{H}_2\text{BDC}$ ) were purchased from J&K Chemical Co. Ltd. (Beijing, China). Montmorillonite KSF was bought from Sigma Ltd (Louis, MO). Phenol, N,N-dimethylformamide,  $\text{H}_2\text{O}_2$  (v/v 30%), methyl orange (MO),  $\text{Fe}(\text{NO}_3)_3 \cdot 9\text{H}_2\text{O}$ , and ethanol were from Sinopharm Chemical Reagent Co. Ltd. (Shanghai, China). HPLC-grade acetonitrile was supplied by Fisher Scientific (Fair Lawn, NJ). All chemicals were used as received without any further purification. Ultrapure water was prepared in the laboratory using a Milli-Q SP reagent water system from Millipore (Milford, MA). Zero-valent iron (ZVI) nanoparticles (50 nm) were obtained from Beijing DK nano technology Co. LTD (Beijing, China). The commercial Fe-C materials were supplied by a plant from Nanjing, Jiangsu province.

### 2.2. Preparation of $\text{Fe}@\text{C}$ -MMT

Fe-metal organic frameworks (Fe-MOFs) were applied both as carbon and iron precursors of  $\text{Fe}@\text{C}$  and prepared using mechanochemical method. Briefly, BDC (0.419 g),  $\text{Fe}(\text{NO}_3)_3 \cdot 9\text{H}_2\text{O}$  (1.212 g), and 8.8 g of 3 mm-diameter zirconia balls were placed in a 50 mL zirconia coated stainless-steel grinding jar and 2 mL of tetramethylammonium hydroxide aqueous solution (v/v 25%) was added. The mixture was milled at 350 rpm using a planetary ball-mill (BM 4, Beijing Grinder Instrument Co., Ltd., Beijing, China). A thick paste was collected after 1 h of grinding. The sample was washed with ethanol and N,N-dimethylformamide three times, and then air-dried at room temperature. The resulting dry sample was brown colored. The obtained Fe-MOF was mixed with montmorillonite KSF with different ratios (2:1, 1:1, 1:2 and 1:3) and then pyrolyzed at 800 °C for 2 h in  $\text{N}_2$  atmosphere to prepare  $\text{Fe}@\text{C}$ -MMT.

### 2.3. Characterization

The morphologies of the synthesized material were inspected on a field-emission scanning electron microscope (FE-SEM, Hitachi S-5500, Tokyo, Japan) and a transmission electron micrograph (TEM, H7500, Hitachi, Japan) operating at 120 kV. The specific surface area was determined by measuring the adsorption/desorption of  $\text{N}_2$  at 77 K using a Micromeritics ASAP 2010 instrument according to the Brunauer–Emmett–Teller (BET) principle. The crystal structure was obtained by X-ray diffraction (XRD) patterns were collected on a PANalytical X'Pert diffractometer (Almelo, Netherlands) using a Cu  $\text{K}\alpha$  radiation ranging from 5° to 70° with a resolution of  $0.02^\circ \text{ min}^{-1}$  scan rate. X-Ray photoelectron spectroscopy (XPS) was measured with an ESCA-Lab-200i-XL spectrometer (Thermo Scientific, Waltham, MA) with monochromatic Al  $\text{K}\alpha$  radiation (1486.6 eV). Fourier transform infrared spectroscopy (FTIR) spectra were recorded in the range of 4000–400  $\text{cm}^{-1}$  by a NEXUS 670 infrared Fourier transform spectrometer (Nicolet Thermo, Waltham, MA) using KBr technique.

### 2.4. Catalytic activity test

Fenton reaction was conducted in 100 mL PET bottles with a vibrating speed of 300 rpm at about 20 °C.  $\text{Fe}@\text{C}$ -MMT catalysts (0.5 g  $\text{L}^{-1}$ ) were first dispersed into 50 mL water containing 100 mg  $\text{L}^{-1}$  of phenol or 50 mg  $\text{L}^{-1}$  of methyl orange (MO). The function of IME on pollutants removal was evaluated by degrading pollutants under aerobic (bubbling with  $\text{O}_2$ ) and anoxic (bubbling with  $\text{N}_2$ ) conditions without addition of  $\text{H}_2\text{O}_2$  at initial pH 4. In IME-Fenton system, the reaction was initiated by adding a known concentration of  $\text{H}_2\text{O}_2$  to the mixture. 0.5 mL of reaction solution were sampled at given time intervals and quenched with 0.5 mL pure ethanol. The solution was analyzed after magnetic separation. Effect of initial solution pH (pH 3–6.5), dosage of catalysts (0.5–2.0 g  $\text{L}^{-1}$ ) and  $\text{H}_2\text{O}_2$  (1–10 mM) on degradation efficiency of MO and phenol was studied. Comparison study was conducted with activated, MMT, ZVI,  $\text{Fe}@\text{C}$  and a commercial Fe-C material under the same experimental condition. All the experiments were conducted in triplicate, and the average values were provided in the figures.

Wastewater sample from a chemical plant in Hebei province was collected to assess the application potential of  $\text{Fe}@\text{C}$ -MMT. The initial concentration of TOC was 307 mg  $\text{L}^{-1}$ . The solution pH of the wastewater was adjusted to pH 4 using diluted HCl and NaOH. The volume of sample and dose of catalyst was 50 mL and 1.0 g  $\text{L}^{-1}$ , respectively, and the concentration of  $\text{H}_2\text{O}_2$  was 30, 50 or 80 mM. The suspension was stirred at 300 rpm. After reaction for 7 h, TOC of the sample was measured.

## 2.5. Sample analysis

The concentration of phenols was measured using Dionex Summit HPLC (Dionex, Sunnyvale, CA) with a PDA-100 photodiode array detector and a DiKMA C<sub>18</sub> column (5  $\mu$ m, 4.6  $\times$  250 mm). The mobile phase was composed of acetonitrile and water (49:51, v/v) at a flow rate of 1.0 mL min<sup>-1</sup>, the detection wavelength and column temperature was set at 280 nm and 30 °C, respectively. The concentration of leaching iron and aluminum from catalysts was analyzed by Inductively Coupled Plasma Mass Spectrometry (ICP-MS, Agilent, CA). The concentration of Fe<sup>2+</sup> and H<sub>2</sub>O<sub>2</sub> were measured spectrophotometrically by the 1,10-phenanthroline and titanium sulfate method, respectively, using a S-3100 UV-vis spectrophotometer. TOC was measured by TOC/TN analyzer (liquic TOC II) (Elementar Corporation, Germany) with deionized water and 0.8% HCl as mobile phase.

## 3. Results and discussion

### 3.1. Characterization of Fe@C-MMT catalysts

In the pyrolysis of MOF, some dissolved carbon precipitate outward in the form of graphitic layers and closely encapsulate the magnetic Fe/Fe<sub>3</sub>C particles to form the core-shell structure [30,31]. In this study, core/shell type Fe@C nanoparticles (NPs) with diameter ranged in 10–50 nm-in-diameter were observed to evenly distribute among the layers of MMT (Fig. 1A and B). SEM images of Fe@C-MMT prepared with different Fe-MOF and MMT ratios showed that Fe@C NPs immobilized and interwove between the layers of MMT (Fig. 1C-F), which avoided aggregation of Fe@C NPs. The crystalline structure of MMT became loose remarkably due to the inserting of Fe@C with the ratio of Fe-MOF and MMT of 2:1, 1:1 and 1:2 (Fig. 1C-E). As the ratio decreased to 1:3, the inserting of Fe@C NPs between the layers of MMT was hardly observed (Fig. 1F). The XRD patterns (Fig. 2A) indicated that the Fe@C-MMT prepared with different Fe-MOF and MMT ratios were composed of MMT, Fe<sup>0</sup> and Fe<sub>3</sub>C [29–32]. Fe<sub>3</sub>C phase usually exists

when Fe metal is synthesized with pyrolysis method at temperature < 1100 °C. The Fe<sub>3</sub>C phase not only acts as excellent Fenton catalysts for degradation of organic pollutants [33–35], but also can promote the IME due to the potential difference between Fe<sup>0</sup> (anode) and Fe<sub>3</sub>C (cathode). The diffraction peak at 20 8.89° [001], reflecting the basal spacing of MMT, was shifted to lower angle 8.84° (Fe@C-MMT (1:1) and Fe@C-MMT (1:2)) and 8.86° (Fe@C-MMT (1:3)), which suggested the increasing basal spacing d001 due to the insertion of Fe@C in the interlayer space of the MMT structure. For Fe@C-MMT (2:1), the reflections for MMT decreased in intensity or disappeared resulting from its low content. Compared to the raw MMT, the insertion of Fe@C enhanced the specific surface areas from 14.7 to 39.8, 48.2, 80.2 and 91.7 m<sup>2</sup>/g for Fe@C-MMT prepared with the ratio of precursors Fe-MOF and MMT was 1:3, 1:2, 1:1 and 2:1, respectively.

The surface properties of these Fe@C-MMT nanocomposites were studied by FTIR and XPS analysis. In the FTIR spectrum of MMT (Fig. 2B), the band near 3630 cm<sup>-1</sup> had been assigned to the stretching vibration of structural OH groups attached to either Al<sup>3+</sup> or Mg<sup>2+</sup>, and the strong adsorption peaks at about 3450 and 1638 cm<sup>-1</sup> were related with the stretching vibration of hydroxyl groups and adsorbed H<sub>2</sub>O on surface or interlayers. In the 700–1500 cm<sup>-1</sup> region, the absorption bands in this region were associated with stretching vibrations of Si-O and Si-O-Si bonds, and also deformation modes of OH groups attached to various ions, e.g., Al<sup>3+</sup>, Mg<sup>2+</sup> and Fe<sup>3+</sup>. The two bands observed at 521 and 469 cm<sup>-1</sup> were related with the stretching vibrations of Si-O-Al or Al-O [23,32,36]. For all Fe@C-MMT nanocomposites, the bands for stretching vibration of OH groups and sorbed water decreased greatly, indicating the elimination of OH groups and increasing of hydrophobicity of the composites surface during pyrolysis. The new peaks at 1580 cm<sup>-1</sup> and 1490 cm<sup>-1</sup> were ascribed to the stretching vibration of C=C and C–H, which were the skeletal vibrations of graphite carbon [37,38], and the bands for Si-O-Al or Al-O were still observed in the Fe@C-MMT samples (Fig. S1).

The high resolution O1s (Fig. 2C) and C1s XPS lines (Fig. S2A) of MMT indicated high content of O atoms on its surface which was mainly

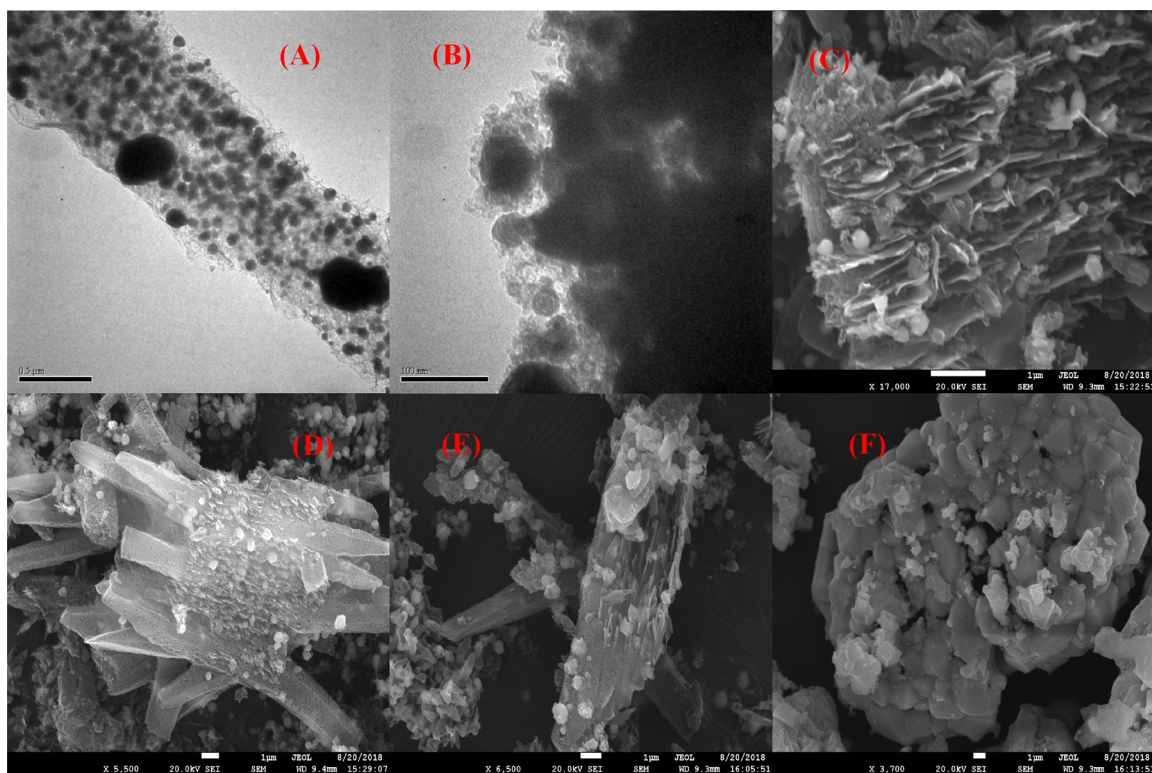


Fig. 1. TEM image (A, B) of Fe@C-MMT (1:1), SEM image of Fe@C-MMT (2:1) (C), Fe@C-MMT (1:1) (D), Fe@C-MMT (1:2) (E), and Fe@C-MMT (1:3) (F).

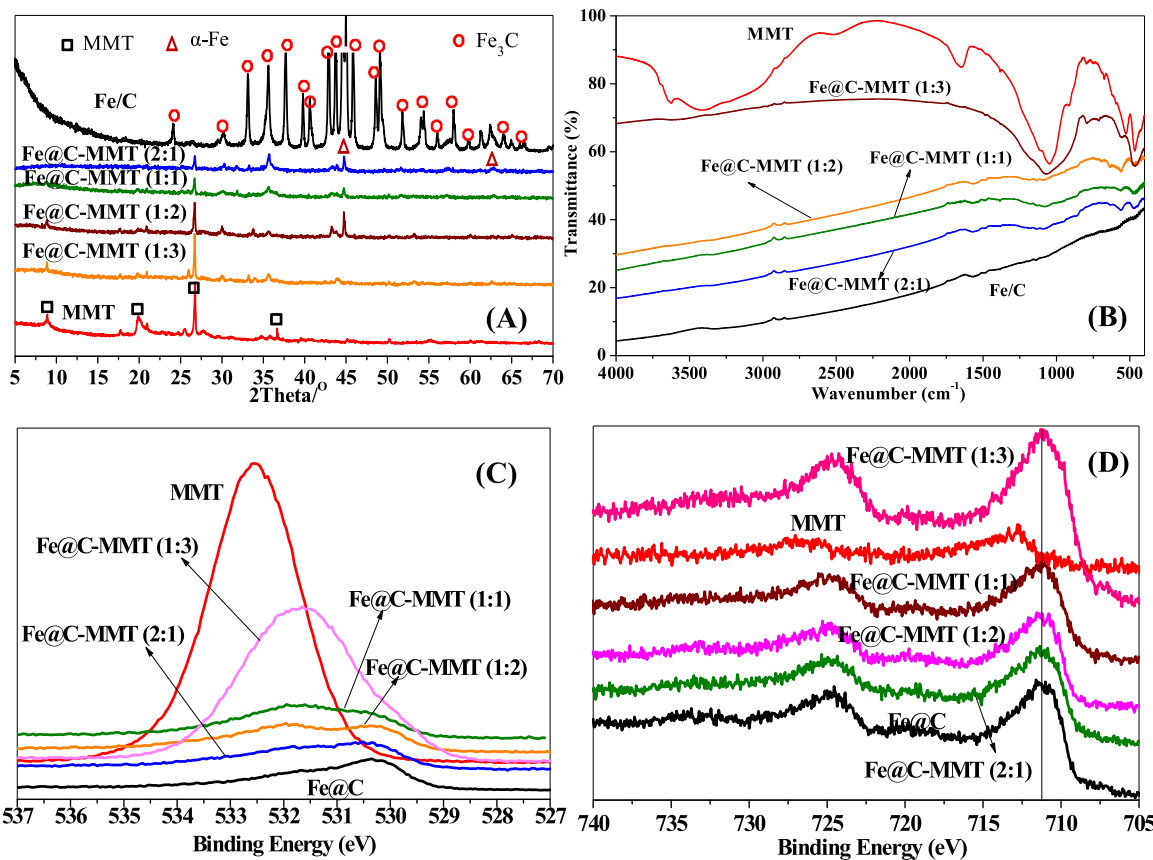


Fig. 2. XRD patterns (A), FTIR spectra (B), O1s XPS spectra (C) and Fe 2p XPS spectra (D) of MMT, Fe@C and Fe@C-MMT nanocomposites.

composed of hydroxyl groups, adsorbed  $\text{H}_2\text{O}$  and  $\text{CO}_3^{2-}$  species. In the surface of Fe@C-MMT composites, the content of O decreased greatly and C increased correspondingly, and M—O, hydroxyl groups, and carboxyl groups, and C—C were the main species. In the Si 2p spectra of these materials (Fig. S2B), the binding energy of Si 2p shifted to low values after pyrolysis with MOF compared to MMT, indicating the formation of low valent Si (such as  $\text{Si}^{3+}$ ,  $\text{Si}^{2+}$  or  $\text{Si}^0$ ) [39], but the signal intensity of Si 2p was much lower than that of MMT. The Fe 2p spectra (Fig. 2D) show that iron atom existed as  $\text{Fe}^0$  in Fe@C-MMT nanocomposites. The amount of iron in MMT, Fe@C, Fe@C-MMT (2:1), Fe@C-MMT (1:1), Fe@C-MMT (1:2) and Fe@C-MMT (1:3) evaluated from the X-ray fluorescence spectrometer was 8.38, 57.2, 48.7, 45.2, 42.8 and 12.4 wt %, respectively. According to the XPS, elemental analysis, ICP-MS and XRF results, the elemental composition of MMT, Fe@C, Fe@C-MMT (2:1), Fe@C-MMT (1:1), Fe@C-MMT (1:2) and Fe@C-MMT (1:3) was Si22.6Al13.7Fe3.2O60.5; Fe23.4C62.4O14.3, Si4.7Al2.8-Fe19.5C57.8O15.2, Si6.8Al4.2Fe18.0C55.7O15.3, Si7.4Al3.6Fe16.6C54.9O17.5, and Si14.6Al8.7Fe4.0C15.2O57.5, respectively.

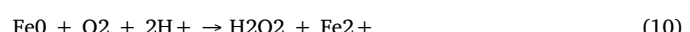
### 3.2. Role of IME and adsorption on phenol and MO removal

In a preliminary study, the catalytic performance of Fe@C-MMT prepared with different MOF and MMT ratios was tested by degrading 100 mg  $\text{L}^{-1}$  of phenol or 50 mg  $\text{L}^{-1}$  of MO at initial pH 4, respectively. The initial concentration of  $\text{H}_2\text{O}_2$  for phenol and MO was 20 mM and 5 mM, respectively. When Fe@C-MMT (1:3) was used as catalyst, the degradation efficiency of phenol and MO was 45% and 60% within 7 h, respectively (Fig. S3). Completely degradation of phenol and MO was achieved when Fe@C-MMT (2:1), Fe@C-MMT (1:1) and Fe@C-MMT (1:2) were used as catalyst in 7 h. But the two pollutants in Fe@C-MMT (1:1)- $\text{H}_2\text{O}_2$  system eliminated much faster than in other systems. Therefore, only the work on Fe@C-MMT (1:1) was mentioned in the

following experiment, and Fe@C-MMT (1:1) labeled as Fe@C-MMT.

Without addition of  $\text{H}_2\text{O}_2$ , the elimination of phenol ranged in 8–13% in Fe@C and Fe@C-MMT suspension at initial solution pH 3.0–6.5 (Fig. 3A) after reaction for 12 h. The removal efficiency of MO was 90%, 83%, 30% and 23%, and 49%, 40%, 20% and 15% treated with Fe@C and Fe@C-MMT at initial pH 3.0, 4.0, 5.5 and 6.5, respectively (Fig. 3B). Phenol can be removed by these materials through surface adsorption and oxidation by the reactive oxygen species (ROS) generated in IME reaction. The removal of MO can proceed via surface adsorption, reduction by  $\text{Fe}^0$  and oxidation [40,41]. To judge the role of each interaction on MO and phenol elimination by Fe@C-MMT, comparison study with activated carbon, MMT and ZVI was conducted at initial pH 4. As a result, the removal efficiencies of phenol were about 10% by these materials and similar with those achieved by Fe@C and Fe@C-MMT. For MO, the removal efficiency was 100%, 82% and 30% within 12 h in activated carbon, MMT and ZVI solution, respectively. These results suggested the important function of surface adsorption for MO removal in IME reaction.

The contribution of  $\text{Fe}^0$  reduction and oxidation by in-situ generated ROS on MO and phenol removal was further evaluated by degrading pollutants under aerobic (bubbling with  $\text{O}_2$ ) and anoxic (bubbling with  $\text{N}_2$ ) conditions. The initial solution pH was adjusted to 4.0. The aerobic condition was beneficial for the in-situ generation of  $\text{H}_2\text{O}_2$  both in ZVI and IME system. Under aerobic conditions, the dissolved oxygen could be reduced into  $\text{H}_2\text{O}_2$  in ZVI system at pH < 5 through two-electron reactions, accompanied with the release of  $\text{Fe}^{2+}$  (Eq. (10)). Subsequently, the released  $\text{Fe}^{2+}$  reacts with  $\text{O}_2$  to produce  $\text{H}_2\text{O}_2$  via a sequential single-electron reduction molecular oxygen activation pathway (Eqs. (11) and (12)) [42,43].



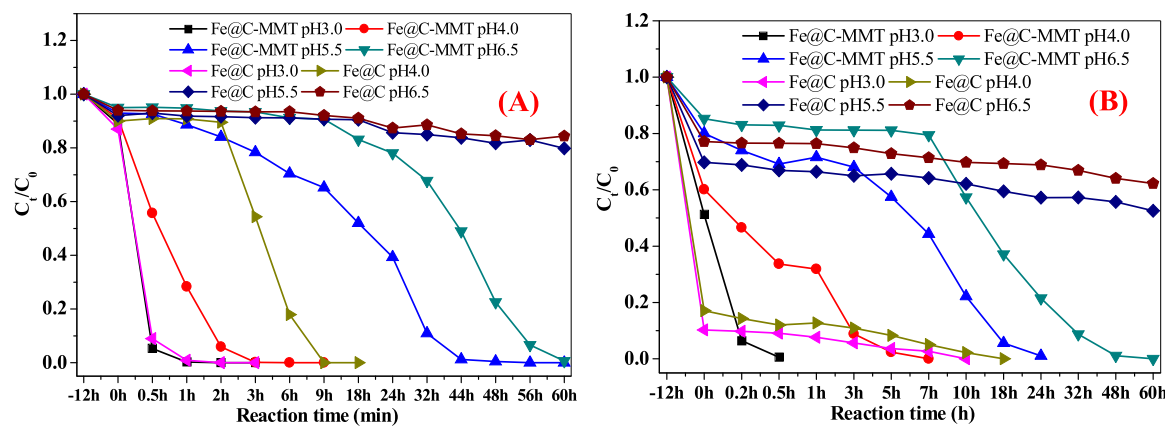
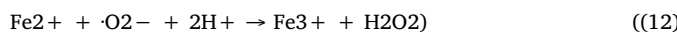


**Fig. 3.** IME-Fenton degradation of phenol (A) and MO (B) catalyzed by Fe@C and Fe@C-MMT at different initial solution pH. Initial concentration of phenol  $100 \text{ mg L}^{-1}$ , MO  $50 \text{ mg L}^{-1}$ , concentration of  $\text{H}_2\text{O}_2$   $20 \text{ mM}$  for phenol and  $5 \text{ mM}$  for MO, dosage of catalyst  $0.5 \text{ g L}^{-1}$ .



Compared with the results without bubbling oxygen, the removal efficiency of phenol increased from 9% to 40% by Fe@C-MMT and from 10% to 25% by ZVI, respectively. The elimination of MO was enhanced from 40% to 76% by Fe@C-MMT, and from 30% to 50% by ZVI after bubbling into oxygen for 12 h (Fig. 4A). This result suggested the possible oxidation of pollutants caused by ROS generated from activation of molecular oxygen by  $\text{Fe}^0$ . The oxidation ability of Fe@C-MMT suspension was clearly superior to the ZVI system due to the fact that the carbon cathode in IME system can catalyze reduction of oxygen to in-situ generate ROS. In anoxic condition without addition of  $\text{H}_2\text{O}_2$ , phenol did not degrade, but complete decolorization of  $50 \text{ mg L}^{-1}$  of MO solution was realized within 12 h (Fig. 4B), resulting from the reduction of MO by  $\text{Fe}^0$ . The higher decolorization efficiency of MO in  $\text{N}_2$  solution than in  $\text{O}_2$  solution indicated that reduction by  $\text{Fe}^0$  took an important role on MO elimination both by ZVI and Fe@C-MMT.

### 3.3. Effect of solution pH, $\text{H}_2\text{O}_2$ concentration and catalyst amount

With the addition of  $\text{H}_2\text{O}_2$ , the degradation of phenol and MO increased obviously catalyzed by Fe@C at initial solution pH 3 and 4 and by Fe@C-MMT in the whole initial pH range (Fig. 3). At initial pH 5.5 and 6.5, the elimination of phenol in Fe@C- $\text{H}_2\text{O}_2$  system was lower than 20% (Fig. 3A). The rate constant for the degradation of phenol and MO was assessed by the pseudo-first-order kinetics. As shown in Fig. 5A and C, the rate constant ( $k_{\text{obs}}$ ) of phenol was  $22.5$  and  $4.16 \text{ L g}^{-1} \text{ h}^{-1}$  and C, the rate constant ( $k_{\text{obs}}$ ) of phenol was  $22.5$  and  $4.16 \text{ L g}^{-1} \text{ h}^{-1}$  catalyzed by Fe@C-MMT at initial pH 3 and 4, and  $17.9 \text{ L g}^{-1} \text{ h}^{-1}$  catalyzed by Fe@C-MMT at initial pH 3 and 4, and  $17.9 \text{ L g}^{-1} \text{ h}^{-1}$

catalyzed by Fe@C at initial pH 3. At initial pH 4, a 2 h of lag period was observed catalyzed by Fe@C (Fig. 3A) and the followed  $k_{\text{obs}}$  value was  $0.81 \text{ L g}^{-1} \text{ h}^{-1}$  (Fig. 5A). The  $k_{\text{obs}}$  values for residual MO at initial pH 3 and 4 were  $18.0$  and  $1.25 \text{ L g}^{-1} \text{ h}^{-1}$  in the Fe@C-MMT- $\text{H}_2\text{O}_2$  system, and  $0.20$  and  $0.18 \text{ L g}^{-1} \text{ h}^{-1}$  in the Fe@C- $\text{H}_2\text{O}_2$  system (Fig. 5C). At initial pH 5.5 and 6.5,  $k_{\text{obs}}$  value for phenol and MO in the Fe@C- $\text{H}_2\text{O}_2$  system was very low (Fig. 5B and D). For phenol, a two-stage kinetic composed of an initial slow degradation stage (first-stage,  $k_{\text{obs}} = 0.11$  and  $0.02$  at initial pH 5.5 and 6.5 respectively) and a followed rapid degradation stage (second-stage,  $k_{\text{obs}} = 0.37$  and  $0.53$  at initial pH 5.5 and 6.5 respectively) for degradation was observed in the Fe@C-MMT- $\text{H}_2\text{O}_2$  system. With regard to MO, a 5 h and 7 h of lag period existed in the Fe@C-MMT- $\text{H}_2\text{O}_2$  system and the followed  $k_{\text{obs}}$  values was  $0.42$  (pH 5.5) and  $0.21$  (pH 6.5)  $\text{L g}^{-1} \text{ h}^{-1}$ , respectively. One possible reason of lag period or lower  $k_{\text{obs}}$  of first stage was the low concentration of dissolved  $\text{Fe}^{2+}$  in the beginning of the reaction (discussed in 3.4). On the other hand, solution pH decreased gradually in the reaction process at different initial pHs (Fig. 5E). This observation has been reported as MMT was used as Fenton or photo-Fenton catalysts [24,26–28]. Some researchers attributed this to the production of organic acids degradation intermediates [26,27]. Actually, at  $\text{pH} \geq 3$ , MMT can continuously release small amount of Al and Si from active surface sites into water in the aging process followed by hydrolysis of dissolved species and secondary precipitation, which resulted in decrease of solution pH [44]. In the present study, the decrease of solution pH was independent on pollutants concentration, which confirmed that self-adjustment of pH was due to the presence of MMT. Thereby, another reason for the two-stage kinetics for phenol degradation in Fe@C-

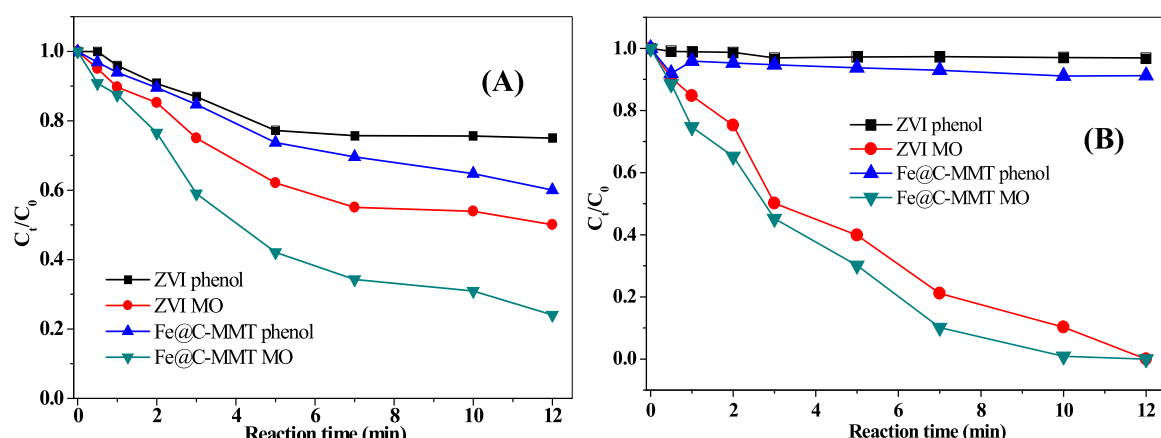


**Fig. 4.** Degradation of phenol and MO catalyzed by Fe@-MMT and ZVI under aerobic (A) and anoxic (B) conditions without the addition of  $\text{H}_2\text{O}_2$ . Initial concentration of phenol  $100 \text{ mg L}^{-1}$ , MO  $50 \text{ mg L}^{-1}$ , dosage of catalyst  $0.5 \text{ g L}^{-1}$ , initial solution pH = 4.

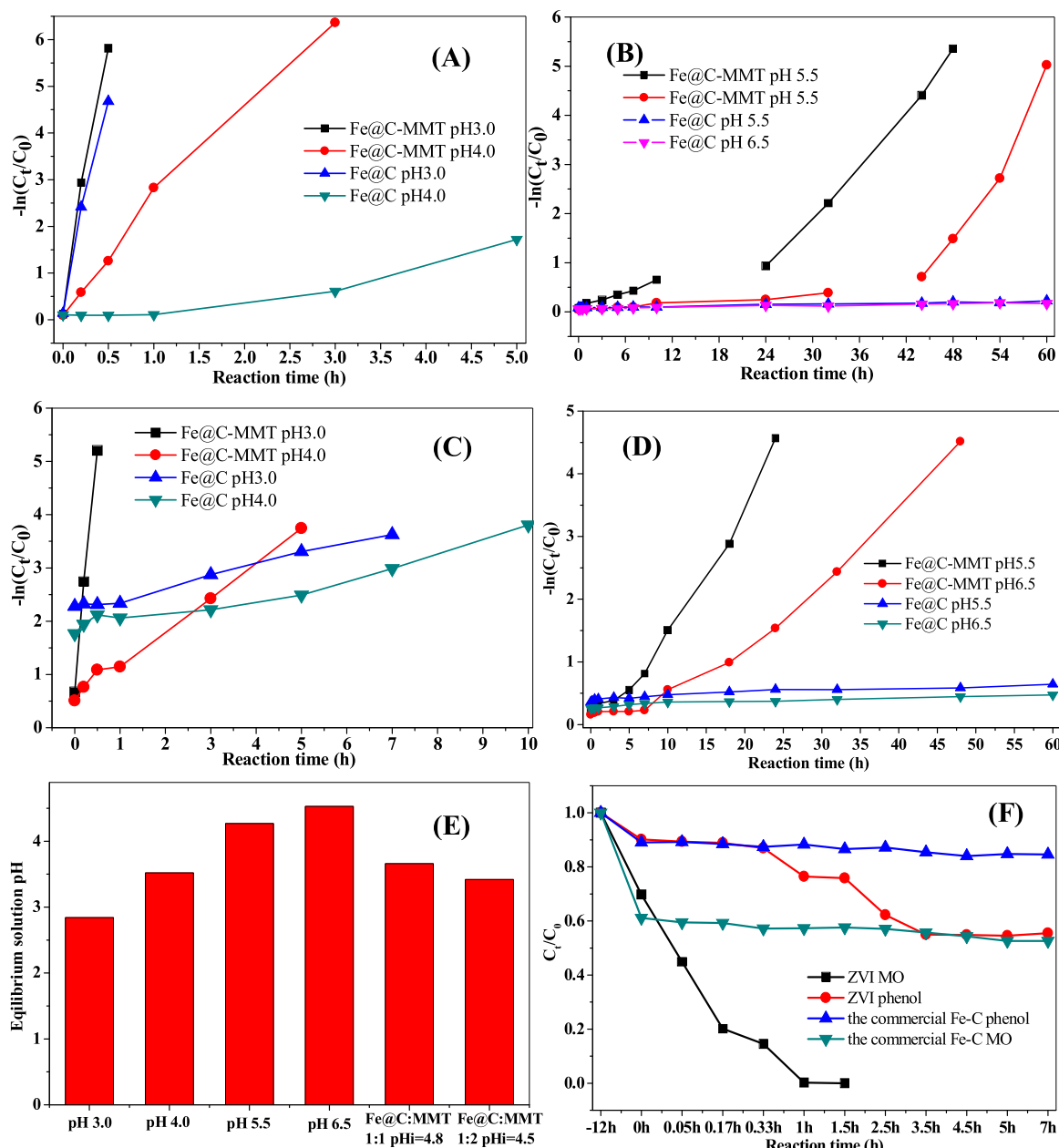


**Fig. 5.** Linear correlation of pseudo-first-order kinetics for IME-Fenton degradation of phenol (A, B) and MO (C, D) catalyzed by Fe@C-MMT and Fe@C at different initial solution pH, change of pH of Fe@C-MMT-H<sub>2</sub>O<sub>2</sub> reaction solution at different initial pH (E), and degradation of phenol and MO catalyzed by ZVI and the commercial Fe-C at initial pH 4 (F). In E dosage of Fe@C:MMT 1:1 0.5 g L<sup>-1</sup> Fe@C + 0.5 g L<sup>-1</sup> of MMT, Fe@C:MMT 1:2 0.5 g L<sup>-1</sup> Fe@C + 1.0 g L<sup>-1</sup> of MMT; dosage of other catalyst 0.5 g L<sup>-1</sup>, MO 50 mg L<sup>-1</sup>, phenol 100 mg L<sup>-1</sup>, concentration of H<sub>2</sub>O<sub>2</sub> for phenol 20 mM, for MO 5 mM.

MMT-H<sub>2</sub>O<sub>2</sub> system should be the dropping of solution pH with reaction time. At initial pH 3 and 4, phenol degradation in the two reaction systems was significantly faster than MO, which may be caused by the strong affinity of MO on the two catalysts that occupied the active sites to slow down Fenton reaction.

At initial pH 3–6.5, the mineralization efficiency of phenol and MO catalyzed by Fe@C-MMT was ranged in 73–85% and 79–84%, respectively (Fig. S4). The superiority of Fe@C-MMT to ZVI and the commercial Fe/C was also investigated. At initial pH 4, ZVI led to fast degradation of MO, but poor oxidative removal of phenol (37%); the commercial Fe-C showed weak catalytic activity for phenol (15%) and MO (45%) elimination (Fig. 5F).

The effect of Fe@C-MMT dosage (0.5–2 g L<sup>-1</sup>) on MO removal was examined. The degradation rate of MO enhanced with the dosage of catalyst. The apparent rate constant at initial pH 4 for the degradation

of MO was 1.25, 0.80, 1.06 and 1.20 L g<sup>-1</sup> h<sup>-1</sup> catalyzed by 0.5, 1.0, 1.5 and 2.0 g L<sup>-1</sup> of Fe@C-MMT in the presence of 5 mM of H<sub>2</sub>O<sub>2</sub>, respectively (Fig. S5A).

The influence of initial concentration of H<sub>2</sub>O<sub>2</sub> on MO degradation was tested with fixed Fe@C-MMT dosage (0.5 g L<sup>-1</sup>) and MO concentration (50 mg L<sup>-1</sup>) at pH 4. With 1 mM of H<sub>2</sub>O<sub>2</sub>, the degradation rate and efficiency (70% in 12 h) of MO was low. Total removal of MO was realized within 9 h as the initial concentration of H<sub>2</sub>O<sub>2</sub> ranged in 3–10 mM and the rate constant was 0.622, 1.25, 1.89 and 2.40 L g<sup>-1</sup> h<sup>-1</sup> for 3, 5, 8 and 10 mM of H<sub>2</sub>O<sub>2</sub>, respectively (Fig. S5B).

### 3.4. Production of Fe<sup>2+</sup> and the role of MMT on Fe<sup>0</sup> corrosion

Due to the interference of MO for detection of Fe<sup>2+</sup> and H<sub>2</sub>O<sub>2</sub> via spectrophotometry method, the kinetic study on Fe<sup>2+</sup> generation and

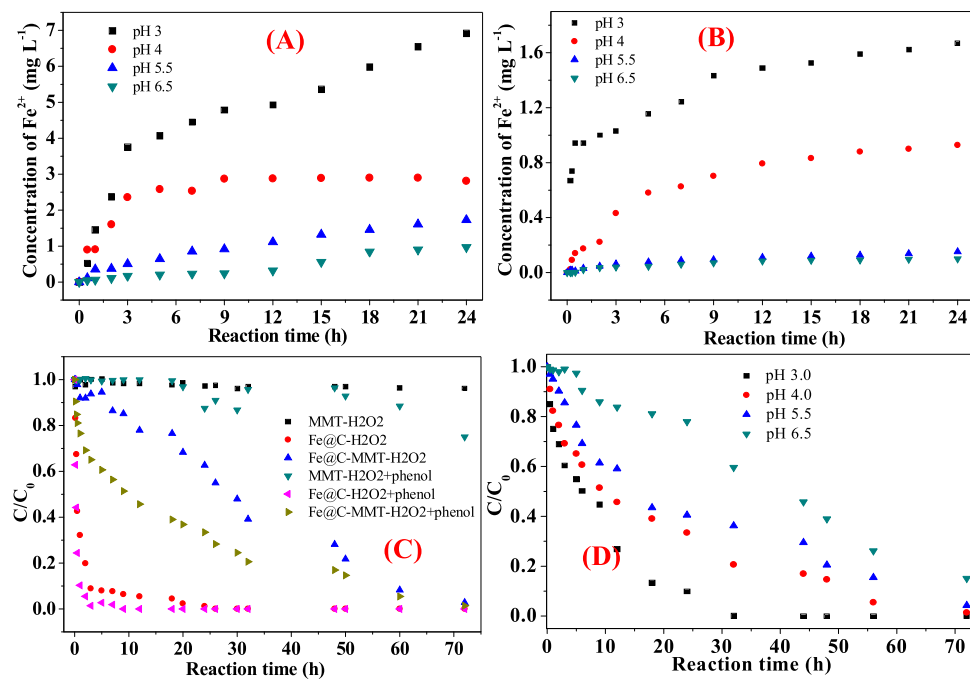
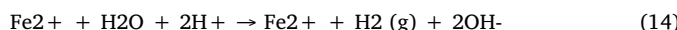
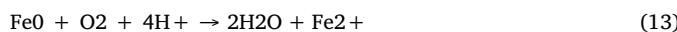


**Fig. 6.** Production of  $\text{Fe}^{2+}$  in reaction process in  $\text{Fe}@\text{C}$ -MMT- $\text{H}_2\text{O}_2$  (A) and  $\text{Fe}@\text{C}$ - $\text{H}_2\text{O}_2$  system (B), consumption of  $\text{H}_2\text{O}_2$  in the presence of different catalysts at initial pH 4 (C), effect of initial solution pH on  $\text{H}_2\text{O}_2$  consumption in  $\text{Fe}@\text{C}$ -MMT- $\text{H}_2\text{O}_2$  system (D). Concentration of phenol  $100 \text{ mg L}^{-1}$ ,  $\text{H}_2\text{O}_2$   $20 \text{ mM}$ .

$\text{H}_2\text{O}_2$  disappearance was conducted by using phenol as model pollutants. In the  $\text{Fe}@\text{C}$  and  $\text{Fe}@\text{C}$ -MMT suspension in the presence of  $\text{H}_2\text{O}_2$ , the concentration of dissolved  $\text{Fe}^{2+}$  increased slowly with reaction time. Within 7 h, the concentrations of  $\text{Fe}^{2+}$  and total Fe ions were  $4.55$ ,  $2.57$ ,  $0.83$  and  $0.20 \text{ mg L}^{-1}$  (Fig. 6A) and  $4.86$ ,  $2.69$ ,  $0.87$  and  $0.28 \text{ mg L}^{-1}$  in  $\text{Fe}@\text{C}$ -MMT suspension at initial pH 3, 4, 5.5 and 6.5, respectively, which was significantly higher than those in the  $\text{Fe}@\text{C}$  suspension ( $1.24$ ,  $0.62$ ,  $0.08$  and  $0.06 \text{ mg L}^{-1}$  and  $1.28$ ,  $0.69$ ,  $0.09$  and  $0.07 \text{ mg L}^{-1}$  for  $\text{Fe}^{2+}$  and total Fe ions at initial pH 3, 4, 5.5 and 6.5 within 7 h (Fig. 6B), respectively). At initial pH 4, Fe ions leaching from  $0.5 \text{ g L}^{-1}$  of MMT was  $0.35 \text{ mg L}^{-1}$  within 7 h. According to the iron content of these materials, the ratio of iron at initial pH 4 leached from MMT,  $\text{Fe}@\text{C}$  and  $\text{Fe}@\text{C}$ -MMT within 7 h was  $0.84$ ,  $0.22$  and  $1.13\%$ , respectively. These results suggested that MMT can accelerate the corrosion of  $\text{Fe}^0$ . MMT contains abundant hydroxyl groups, which strongly adsorbs dissolved  $\text{O}_2$  and water molecules [27]. Protons in water are inevitably adsorbed on MMT surface through ion exchange with cations (such as  $\text{Na}^+$ ,  $\text{K}^+$ ) [29]. These reactions provide an oxygen- and  $\text{H}^+$ -rich microenvironment on MMT surfaces, and can accelerate corrosion of  $\text{Fe}^0$  according to Eqs. (13) and (14) [16,42,43]:



The accelerated corrosion of  $\text{Fe}^0$  in  $\text{Fe}@\text{C}$ -MMT may facilitate the in-situ generation of  $\text{Fe}^{2+}$  and  $\text{H}_2\text{O}_2$ , thus improved the subsequent Fenton reaction.

### 3.5. Consumption of $\text{H}_2\text{O}_2$ and long-lasting activity of $\text{Fe}@\text{C}$ -MMT- $\text{H}_2\text{O}_2$ system

In MMT suspension,  $\text{H}_2\text{O}_2$  concentration is nearly constant in the absence of phenol within 72 h at  $20^\circ\text{C}$ , suggesting the inert nature of MMT surface and low catalytic activity of MMT for  $\text{H}_2\text{O}_2$  decomposition. In  $\text{Fe}@\text{C}$  suspension (Fig. 6C),  $\text{H}_2\text{O}_2$  decomposed rapidly with the pseudo-second order constant was  $0.838 \text{ mM h}^{-1}$ . Compared to  $\text{Fe}@\text{C}$ ,  $\text{Fe}@\text{C}$ -MMT catalysts retarded decomposition of  $\text{H}_2\text{O}_2$  greatly ( $0.018 \text{ mM h}^{-1}$ ). The addition of phenol led to 25% of  $\text{H}_2\text{O}_2$

disappearance in MMT suspension, and increased the consumption rate of  $\text{H}_2\text{O}_2$  in the  $\text{Fe}@\text{C}$  and  $\text{Fe}@\text{C}$ -MMT suspension ( $0.987 \text{ mM h}^{-1}$  and  $0.046 \text{ mM h}^{-1}$  for  $\text{Fe}@\text{C}$  and  $\text{Fe}@\text{C}$ -MMT, respectively).

We have mentioned that the MMT coat promoted the corrosion of  $\text{Fe}^0$  in  $\text{Fe}@\text{C}$ -MMT compared to  $\text{Fe}@\text{C}$ . However, the consumption of  $\text{H}_2\text{O}_2$  by  $\text{Fe}@\text{C}$  was still faster than by  $\text{Fe}@\text{C}$ -MMT. This can be explained by two possible reasons. Firstly, the concentration of released  $\text{Fe}^{2+}$  in  $\text{Fe}@\text{C}$ -MMT reaction solution was not high enough due to the low content of MMT in the nanocomposite. If  $\text{Fe}@\text{C}$ , ZVI and the commercial  $\text{Fe}/\text{C}$  material was physically mixed with raw MMT (2:1 to 1:2), the concentration of  $\text{Fe}^{2+}$  released to reaction solution was 16–25, 4.5–5.3, and 14–18 times compared to that of  $\text{Fe}@\text{C}$ , ZVI, and the commercial  $\text{Fe}/\text{C}$  system, respectively (Table S1). At the same time, 5 mM of  $\text{H}_2\text{O}_2$  totally consumed within 30 min in all the physically mixed materials systems. Secondly, the MMT coat retarded the direct contact of  $\text{Fe}^0$  or surface adsorbed  $\text{Fe}(\text{II})$  species with  $\text{H}_2\text{O}_2$ , which slowed down the decomposition of  $\text{H}_2\text{O}_2$  by  $\text{Fe}(\text{II})$  species on  $\text{Fe}@\text{C}$ -MMT surface.

The initial solution pH affected the elimination rate of  $\text{H}_2\text{O}_2$ . Time for  $\text{H}_2\text{O}_2$  disappearance was 32 h at initial pH 3 and extended to 72 h both at initial pH 4 and pH 5.5. At initial pH 6.5, about 20% of  $\text{H}_2\text{O}_2$  still remained after phenol degradation for 72 h (Fig. 6D). The slow decomposition of  $\text{H}_2\text{O}_2$  and continuous generation of low concentration of  $\text{Fe}^{2+}$  in the reaction process ensured the long-lasting efficiency of the  $\text{Fe}@\text{C}$ -MMT- $\text{H}_2\text{O}_2$  system, which was responsible for the great mineralization rate of pollutants catalyzed by  $\text{Fe}@\text{C}$ -MMT at initial solution pH 5.5 and 6.5.

The long lasting Fenton degradation efficiency of the  $\text{Fe}@\text{C}$ -MMT- $\text{H}_2\text{O}_2$  system was examined by using  $0.5 \text{ g L}^{-1}$  of solid as catalyst and spiking with low concentration of  $\text{H}_2\text{O}_2$  at initial pH 4. The initial concentration of MO and  $\text{H}_2\text{O}_2$  was  $50 \text{ mg L}^{-1}$  and  $10 \text{ mM}$  (67 equiv of  $\text{H}_2\text{O}_2$  with respect to MO), respectively. After decolorization/elimination of MO (about 7 h each run), the MO concentration was adjusted to  $50 \text{ mg L}^{-1}$  again by adding small volume of concentrated MO stores without addition new  $\text{H}_2\text{O}_2$  and adjustment of solution pH. The reaction system kept high activity until MO was re-spiked for five times (Fig. 7A). So the powerful Fenton activity of  $\text{Fe}@\text{C}$ -MMT suspension with low concentration of  $\text{H}_2\text{O}_2$  can sustain about 40 h to continuously

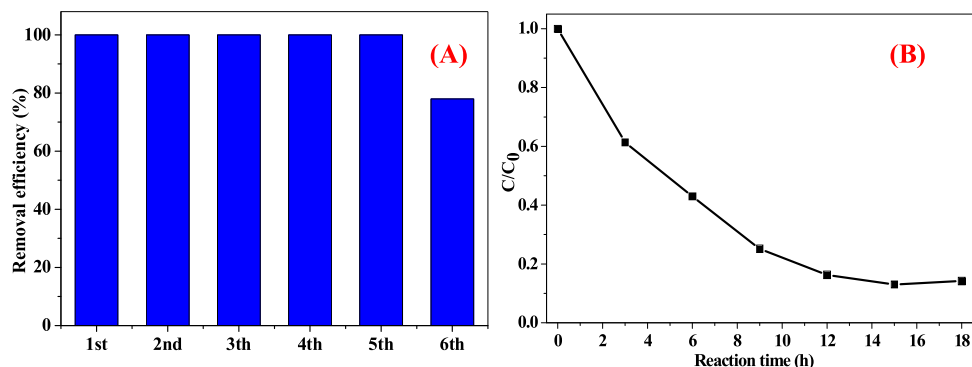


**Fig. 7.** The long-lasting efficiency of Fe@C-MMT-H<sub>2</sub>O<sub>2</sub> for continuous degradation of MO (A), and removal of 1000 mg L<sup>-1</sup> of MO by Fe@C-MMT-H<sub>2</sub>O<sub>2</sub> (B). Initial solution pH 4.0, concentration of spiked MO each time in A: 50 mg L<sup>-1</sup>, H<sub>2</sub>O<sub>2</sub> in A 10 mM, B 40 mM.

degrade organic pollutants. In other words, 250 mg L<sup>-1</sup> of MO could be degraded with 13.3 equiv of H<sub>2</sub>O<sub>2</sub>. If Fe@C was used as Fenton catalyst, MO degradation stopped in the third spike. Regeneration of the Fe@C-MMT-H<sub>2</sub>O<sub>2</sub> system was realized by directly restoring the initial concentration of H<sub>2</sub>O<sub>2</sub> to 10 mM, not necessary to collect and treat the Fe@C-MMT catalyst. The efficiency of the regenerated Fenton reaction system in the second and third run was the same to that of the fresh Fe@C-MMT-H<sub>2</sub>O<sub>2</sub> system. The Fe@C-MMT (0.5 g L<sup>-1</sup>) reaction system was also used to treat high concentration of MO (1000 mg L<sup>-1</sup>) with 13.3 equiv of H<sub>2</sub>O<sub>2</sub> (40 mM) with respect to MO. The results obtained showed that 86% of MO was decomposed at room temperature (Fig. 7B). These results confirmed the excellent catalytic performance of Fe@C-MMT and long-lasting activity of the reaction system, which was contributed by rate-controlling consumption of H<sub>2</sub>O<sub>2</sub> combined with the selective decomposition of H<sub>2</sub>O<sub>2</sub> to ·OH radicals.

### 3.6. Reusability of Fe@C-MMT

The reusability of Fe@C-MMT was tested by recovering the solid

using magnetic separation technology under a magnet after a 7 h run, washing the solid with DI water and reusing it for a consecutive run. After reused for 5 cycles, the degradation efficiency of MO reduced progressively. At the tenth use, 80% of MO still could be eliminated. The mineralization efficiency of MO in the ten runs ranged in 58–88%, and the concentration of leached Fe and Al ions was less than 2.5 (0.87% of the Fe element in Fe@C-MMT) and 1.0 mg L<sup>-1</sup>, respectively (Fig. 8A-C). It is worth noting that Fe-C materials are sacrificial catalysts whose catalytic activity inevitably decreased after usage. The good reusability of Fe@C-MMT resulted from its powerful catalytic activity. The reusability of the Fe@C and MMT was also studied, and complete removal of MO only was achieved twice. This can be explained by the fact that MO removal by Fe@C and MMT mostly relied on surface adsorption. The adsorbed MO was hardly further oxidized and occupied the active sites. When all the active sites were taken up by MO, the catalysts were totally deactivated. Owing to the core/shell structure, Fe@C and Fe@C-MMT possessed outstanding resistance to oxygen and acid corrosion. After soaking in reaction solution at pH 4 for three months, the commercial Fe/C and ZVI turned from black to yellow

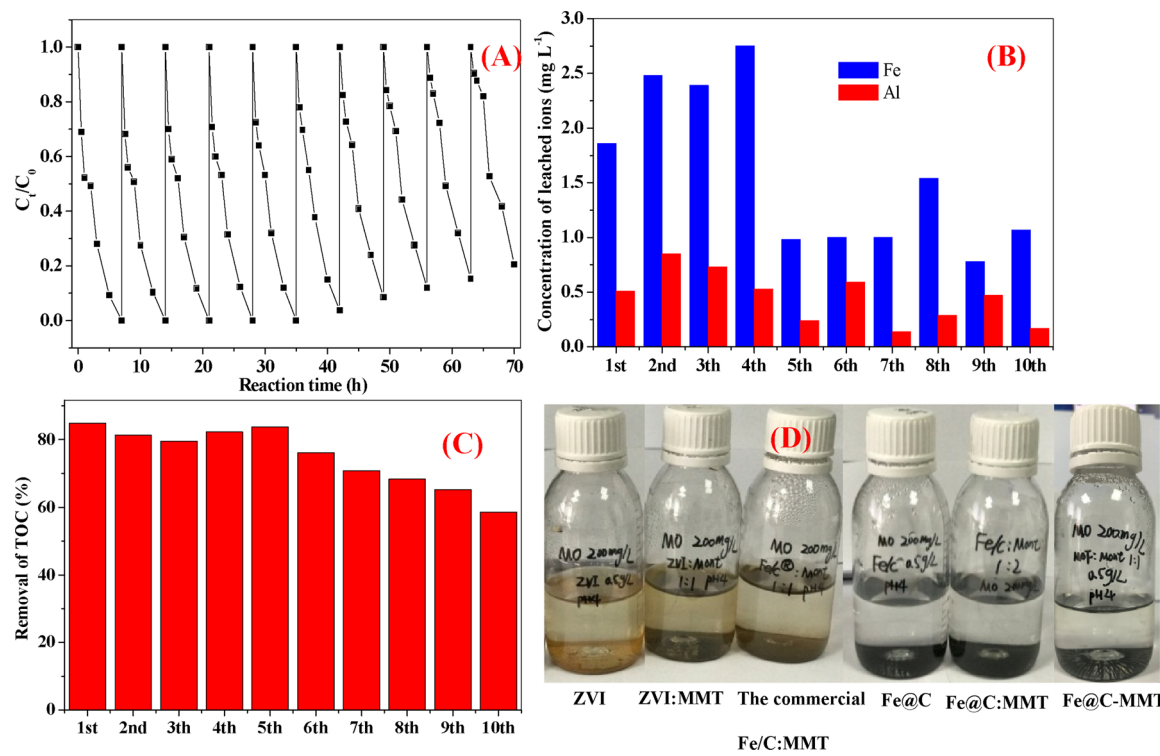


**Fig. 8.** Recycling runs of Fe@C-MMT (A), concentration of leaching Fe and Al ions (B) and removal of TOC (C) in each recycling, and images of different catalysts soaked at pH 4 for three months (D). Initial solution pH = 4, concentration of MO and H<sub>2</sub>O<sub>2</sub>: 50 mg L<sup>-1</sup> and 5 mM, dosage of catalyst: 0.5 g L<sup>-1</sup>.

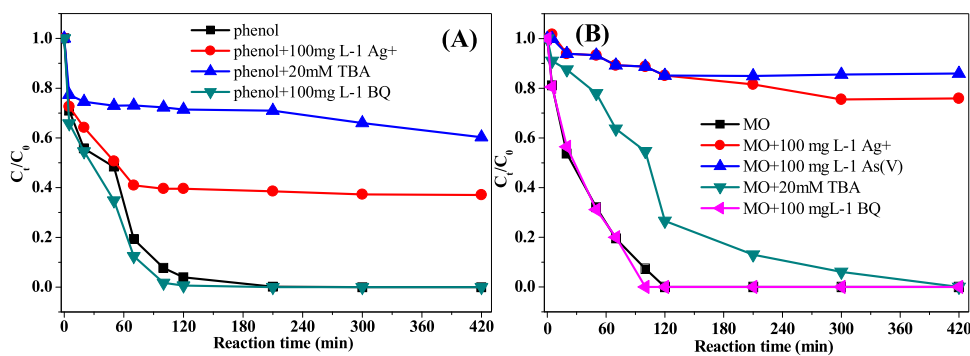


**Fig. 9.** Effect of reactive species inhibitors in Fe@C-MMT-H<sub>2</sub>O<sub>2</sub> system on phenol (A) and MO (B) degradation at initial pH 3.8. Concentration of MO 50 mg L<sup>-1</sup>, phenol 100 mg L<sup>-1</sup>, concentration of H<sub>2</sub>O<sub>2</sub> for phenol 20 mM, for MO 5 mM, dosage of Fe@C-MMT 0.5 g L<sup>-1</sup>.

entirely, however, the Fe@C and Fe@C-MMT catalysts still kept black (Fig. 8D).

### 3.7. Reaction mechanisms

The role of ROS (·OH and HO<sub>2</sub><sup>·</sup>/O<sub>2</sub><sup>·-</sup>) on the degradation of MO and phenol was evaluated by adding t-butyl alcohol and benzoquinone (BQ) as the quencher of ·OH and HO<sub>2</sub><sup>·</sup>/O<sub>2</sub><sup>·-</sup>, respectively. The addition of BQ promoted MO and phenol degradation slightly, which is consistent with the report that BQ posted positive effect on Fenton degradation of organic pollutants (Fig. 9A and B). The presence of t-butyl alcohol did not affect the degradation efficiency of MO, but the degradation rate constant decreased from 2.655 L g<sup>-1</sup> h<sup>-1</sup> to 1.163 L g<sup>-1</sup> h<sup>-1</sup>. For phenol, the degradation efficiency reduced to 40% in the presence of t-butyl alcohol. We utilized Ag<sup>+</sup> and As(V) as quencher of electrons to study the effect of electrons (Fe<sup>0</sup>) on removal of targets. As a result, the addition of 100 mg L<sup>-1</sup> of Ag<sup>+</sup> and 100 mg L<sup>-1</sup> of As(V) reduced the elimination efficiency of MO from 100% to 35% and 15%, respectively. The degradation efficiency of phenol decreased to 60% in the presence of 100 mg L<sup>-1</sup> of Ag<sup>+</sup>. Ag<sup>+</sup> can be reduced by Fe<sup>0</sup> and Fe<sup>2+</sup> to produce Ag NPs [45]. The consumption of Fe<sup>2+</sup> by Ag<sup>+</sup> affected Fenton reaction, leading to decreased removal efficiency of pollutants. Generally, the negative effect of t-butyl alcohol and Ag<sup>+</sup> on phenol degradation suggested the important role of ·OH on its degradation. The removal of arsenic in ZVI/O<sub>2</sub> and ZVI/H<sub>2</sub>O<sub>2</sub> systems are attributed to adsorption and co-precipitation by iron hydroxides generated from the corrosion of Fe<sup>0</sup>, and partly reduction of As(V) to As(III) by Fe<sup>0</sup> also took place [46]. The negative effect of Ag<sup>+</sup> and As(V) on MO removal proved that reduction by Fe<sup>0</sup> and surface adsorption was responsible for fast MO decolorization in Fe@C-MMT-H<sub>2</sub>O<sub>2</sub> system. But the Fenton reaction was fundamental for mineralization of MO from water sample and

“regeneration” of catalysts. The schematic diagram of reaction mechanism was shown in Fig. 10.

### 3.8. Application potential of Fe@C-MMT

We have investigated the application potential of Fe@C-MMT in treatment of wastewater from a chemical industry (Hebei province). The dosage of Fe@C-MMT was 1 g L<sup>-1</sup>, and solution pH was adjusted to pH 4. After reacted for 7 h, the concentration of TOC was decreased from 307 mg L<sup>-1</sup> to 193, 110 and 43 mg L<sup>-1</sup> as the concentration of H<sub>2</sub>O<sub>2</sub> was 30, 50 and 80 mM, respectively. The concentration of leached Fe ions was detected to be about 3 mg L<sup>-1</sup>. This result indicated the reasonable catalytic performance of Fe@C-MMT in wastewater samples.

## 4. Conclusion

Core/shell structured Fe@C nanocomposites were prepared by using Fe-MOF as Fe and C co-precursors. The Fe@C distributed on the surface and inserted between the interlayers of montmorillonite evenly via one-step pyrolysis. The MMT in the Fe@C-MMT nanocomposites contributed to rate-controlling decomposition of H<sub>2</sub>O<sub>2</sub>, and the continuously released Fe<sup>2+</sup> from Fe@C ensured selective decomposition of H<sub>2</sub>O<sub>2</sub> to ·OH radicals. Therefore, the IME-Fenton system can maintain long-lasting activity to achieve high efficient degradation and mineralization of phenol and MO as the initial solution pH was 5.5 and 6.5. Owning to concentrated layers of adsorbed O<sub>2</sub>, H<sub>2</sub>O and H<sup>+</sup> on the surface, MMT could promote corrosion of Fe<sup>0</sup> and in-situ generation of ROS. Therefore, Fe@C-MMT possessed higher catalytic performance for phenol and MO degradation in IME-Fenton reaction system than Fe@C, ZVI and the commercial Fe-C material. Finally, Fe@C-MMT has shown good application potential for wastewater treatment.

## Notes

The authors declare no competing financial interest.

## Acknowledgements

This work was jointly supported by National Key Research and Development Program of China (2016YFA0203100), the National Natural Science Foundation of China (21537004, 21777169, 21621064), and Strategic Priority Research Program of the Chinese Academy of Sciences (XDB14010201).

## Appendix A. Supplementary data

Supplementary material related to this article can be found, in the online version, at doi:<https://doi.org/10.1016/j.apcatb.2019.117820>.

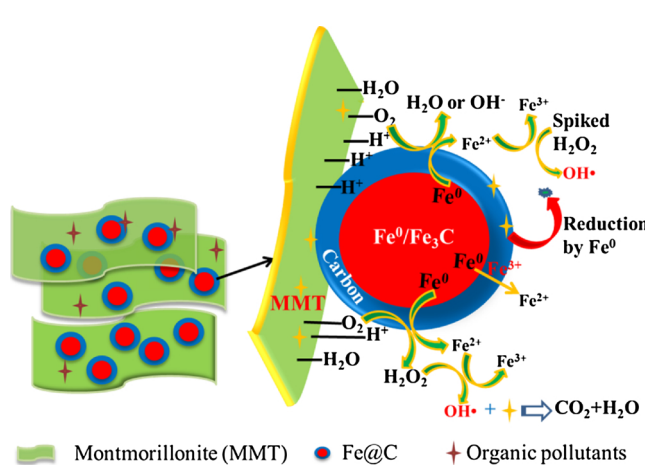


**Fig. 10.** Reaction mechanisms of IME-Fenton on the surface of Fe@C-MMT.

## References

- [1] D.W. Ying, X.Y. Xu, K. Li, Y.L. Wang, J.P. Jia, Design of a novel sequencing batch internal micro-electrolysis reactor for treating mature landfill leachate, *Chem. Eng. Res. Des.* 90 (2012) 2278–2286.
- [2] S. Zhang, D. Wang, L. Zhou, X.W. Zhang, P.P. Fan, X. Quan, Intensified internal electrolysis for degradation of methylene blue as model compound induced by a novel hybrid material: multi-walled carbon nanotubes immobilized on zero-valent iron plates (Fe0-CNTs), *Chem. Eng. J.* 217 (2013) 99–107.
- [3] Q.S. Zhu, S.H. Guo, C.M. Guo, D. Dai, X.K. Jiao, T.Q. Ma, J.F. Chen, Stability of Fe–C micro-electrolysis and biological process in treating ultra-high concentration organic wastewater, *Chem. Eng. J.* 225 (2014) 535–540.
- [4] Y.H. Han, H. Li, M.L. Liu, Y.M. Sang, C.Z. Liang, J.Q. Chen, Purification treatment of dyes wastewater with a novel micro-electrolysis reactor, *Sep. Purif. Technol.* 170 (2016) 241–247.
- [5] Z.M. Yang, Y.P. Ma, Y. Liu, Q.S. Li, Z.Y. Zhou, Z.Q. Ren, Degradation of organic pollutants in near-neutral pH solution by Fe-C micro-electrolysis system, *Chem. Eng. J.* 315 (2017) 403–414.
- [6] Y.Z. Liu, C. Wang, Z.Y. Sui, D.L. Zou, Degradation of chlortetracycline using nano micro-electrolysis materials with loading copper, *Sep. Purif. Technol.* 203 (2018) 29–35.
- [7] X.Y. Zhu, X.J. Chen, Z.M. Yang, Y. Liu, Z.Y. Zhou, Z.Q. Ren, Investigating the influences of electrode material property on degradation behavior of organic wastewaters by iron-carbon micro-electrolysis, *Chem. Eng. J.* 338 (2018) 46–54.
- [8] L.Q. Wang, Q. Yang, D.B. Wang, X.M. Li, G.M. Zeng, Z.J. Li, Y.C. Deng, J. Liu, K.X. Yi, Advanced landfill leachate treatment using iron-carbon microelectrolysis–Fenton process: process optimization and column experiments, *J. Hazard. Mater.* 318 (2016) 460–467.
- [9] H. Zhang, L.J. Xiang, D.B. Zhang, H. Qing, Treatment of landfill leachate by internal microelectrolysis and sequent Fenton process, *Desalin. Water Treat.* 47 (2012) 243–248.
- [10] C. Huang, F. Peng, H.J. Guo, C. Wang, M.T. Luo, C. Zhao, L. Xiong, X.F. Chen, X.D. Chen, Efficient COD degradation of turpentine processing wastewater by combination of Fe-C micro-electrolysis and Fenton treatment: long-term study and scale up, *Chem. Eng. J.* 351 (2018) 697–707.
- [11] X.Q. Wang, X.K. Gong, Q.X. Zhang, H.J. Du, Degradation mechanism of Direct Pink 12B treated by iron-carbon micro-electrolysis and Fenton reaction, *J. Environ. Sci.* 25 (Suppl.) (2013) S63–S68.
- [12] Z.H. Diao, X.R. Xu, D. Jiang, G. Li, J.J. Liu, L.J. Kong, L.Z. Zuo, Enhanced catalytic degradation of ciprofloxacin with FeS2/SiO2 microspheres as heterogeneous Fenton catalyst: kinetics, reaction pathways and mechanism, *J. Hazard. Mater.* 327 (2017) 108–115.
- [13] M. Tokumura, R. Morito, R. Hatayama, Y. Kawase, Iron redox cycling in hydroxyl radical generation during the photo-Fenton oxidative degradation: dynamic change of hydroxyl radical concentration, *Appl. Catal. B* 106 (2011) 565–576.
- [14] S. Zha, Y. Cheng, Y. Gao, Z. Chen, M. Megharaj, R. Naidu, Nanoscale zero-valent iron as a catalyst for heterogeneous Fenton oxidation of amoxicillin, *Chem. Eng. J.* 255 (2014) 141–148.
- [15] J. Wang, C. Liu, J. Li, R. Luo, X. Hu, X. Sun, J. Shen, W. Han, L. Wang, In-situ incorporation of iron-copper bimetallic particles in electrospun carbon nanofibers as an efficient Fenton catalyst, *Appl. Catal. B* 207 (2017) 316–325.
- [16] R. Yamaguchi, S. Kurosu, M. Suzuki, Y. Kawase, Hydroxyl radical generation by zero-valent iron/Cu (ZVI/Cu) bimetallic catalyst in wastewater treatment: heterogeneous Fenton/Fenton-like reactions by Fenton reagents formed in-situ under oxic conditions, *Chem. Eng. J.* 334 (2018) 1537–1549.
- [17] K.J. Datta, M.B. Gawande, K.K.R. Datta, V. Ranc, J. Pechousek, M. Krizek, J. Tucek, R. Kale, P. Pospisil, R.S. Varma, T. Asefa, G. Zoppellaro, R. Zboril, Micro-mesoporous iron oxides with record efficiency for decomposition of hydrogen peroxide: morphology driven catalysis for degradation of organic contaminants, *J. Mater. Chem. A* 4 (2016) 596–604.
- [18] J. Virkutyte, R.S. Varma, et al., Greener and sustainable remediation using iron nanomaterials, in: V. Sharma (Ed.), *Green Catalysts for Energy Transformation and Emission Control*, ACS Symposium Series 1184, American Chemical Society, Washington, D. C, 2014, pp. 1–21 Chapter 1.
- [19] Y.J. Wang, D.A. Jia, R.J. Sun, H.W. Zhu, D.M. Zhou, Adsorption and desorption of tetracycline and copper(II) on montmorillonite as affected by solution pH, *Environ. Sci. Technol.* 42 (2008) 3254–3259.
- [20] S.S. Gupta, K.G. Bhattacharyya, Adsorption of heavy metals on kaolinite and montmorillonite: a review, *Phys. Chem. Chem. Phys.* 14 (2012) 6698–6723.
- [21] C.Y. Deng, C. Ren, F. Wu, N.S. Deng, E.M. Glebov, I.P. Pozdnyakov, V.F. Plyusnin, Montmorillonite KSF as catalyst for degradation of acetaminophen with heterogeneous Fenton reaction, *Reac. Kinet. Mech. Cat.* 100 (2010) 277–288.
- [22] M.F. Zeng, Y.D. Wang, Q. Liu, X. Yuan, S.F. Zuo, R.K. Feng, J. Yang, B.Y. Wang, C.Z. Qi, Y. Lin, Encaging palladium nanoparticles in chitosan modified montmorillonite for efficient, recyclable catalysts, *ACS Appl. Mater. Interfaces* 8 (2016) 33157–33164.
- [23] L. Bian, J.A. Nie, X.Q. Jiang, M.X. Song, F.Q. Dong, W.M. Li, L.P. Shang, H. Deng, H.C. He, B. Xu, B. Wang, X.B. Gu, Selective removal of uranyl from aqueous solutions containing a mix of toxic metal ions using core–shell  $\text{MFe}_2\text{O}_4$ – $\text{TiO}_2$  nanoparticles of montmorillonite edge sites, *ACS Sustainable Chem. Eng.* 6 (12) (2018) 16267–16278.
- [24] M. Bobu, A. Yediler, I. Siminiceanu, S. Schulte-Hostede, Degradation studies of ciprofloxacin on a pillared iron catalyst, *Appl. Catal. B: Environ.* 83 (2008) 15–23.
- [25] J. Virkutyte, R.S. Varma, Eco-friendly magnetic iron oxide-pillared montmorillonite for advanced catalytic degradation of dichlorophenol, *ACS Sustainable Chem. Eng.* 2 (2014) 1545–1550.
- [26] X.P. Wei, H.H. Wu, F. Sun, Magnetite/Fe-Al-montmorillonite as a Fenton catalyst with efficient degradation of phenol, *J. Colloid Inter. Sci.* 504 (2017) 611–619.
- [27] M.J. Jin, M.C. Long, H.R. Su, Y. Pan, Q.Z. Zhang, J. Wang, B.X. Zhou, Y.W. Zhang, Magnetically separable maghemite/montmorillonite composite as an efficient heterogeneous Fenton-like catalyst for phenol degradation, *Environ. Sci. Pollut. Res.* 24 (2017) 1926–1937.
- [28] S.S. Yang, P.X. Wu, Q.L. Yang, N.W. Zhu, G.N. Lu, Z. Dang, Regeneration of iron-montmorillonite adsorbent as an efficient heterogeneous Fenton catalytic for degradation of Bisphenol A: structure, performance and mechanism, *Chem. Eng. J.* 328 (2017) 737–747.
- [29] E. Tombácz, M. Szekeres, Colloidal behavior of aqueous montmorillonite suspensions: the specific role of pH in the presence of indifferent electrolytes, *Appl. Clay Sci.* 27 (2004) 75–94.
- [30] G.M. Li, L.C. Wang, W.X. Li, Y. Xu, Mesoporous Fe/C and core-shell Fe-Fe3C@C composites as efficient microwave absorbents, *Micropor. Mesopor. Mater.* 211 (2015) 97–104.
- [31] R. Qiang, Y.C. Du, H.T. Zhao, Y. Wang, C.H. Tian, Z.G. Li, X.J. Han, P. Xu, Metal organic framework-derived Fe/C nanocubes toward efficient microwave absorption, *J. Mater. Chem. A* 3 (2015) 13426–13434.
- [32] K. Kalantari, M.B. Ahmad, K. Shameli, M.Z.B. Hussein, R. Khandanlou, H. Khanehzaei, Size-controlled synthesis of  $\text{Fe}_3\text{O}_4$  magnetic nanoparticles in the layers of montmorillonite, *J. Nanomater.* 2014 (2014) 739485.
- [33] J.J. Shi, Y.Y. Wang, Weichen Du, Z.Y. Hou, Synthesis of graphene encapsulated Fe3C in carbon nanotubes from biomass and its catalysis application, *Carbon* 99 (2016) 330–337.
- [34] G.L. Zhang, Y.B. Ding, W.S. Nie, H.Q. Tang, Efficient degradation of drug ibuprofen through catalytic activation of peroxymonosulfate by Fe3C embedded on carbon, *J. Environ. Sci.* 78 (2019) 1–12.
- [35] Q. Peng, Y.B. Ding, L.H. Zhu, G.L. Zhang, H.Q. Tang, Fast and complete degradation of norfloxacin by using Fe/Fe3C@NG as a bifunctional catalyst for activating peroxymonosulfate, *Sep. Purif. Technol.* 202 (2018) 307–317.
- [36] I. Fatimah, D. Rubiyanto, T. Huda, Effect of sulfation on zirconia-pillared montmorillonite to the catalytic activity in microwave-assisted citronellal conversion, *Int. J. Chem. Eng.* 2014 (2014) 950190.
- [37] Y.N. Sudhakar, M. Selvakumar, D. Krishna Bhat, S. Senthil Kumar, Reduced graphene oxide derived from used cell graphite and its green fabrication as an eco-friendly supercapacitor, *RSC Adv.* 4 (2014) 60039–60051.
- [38] J.J. Prias-Barragan, K. Gross, H. Ariza-Calderon, P. Prieto, Synthesis and vibrational response of graphite oxide platelets from bamboo for electronic applications, *Phys. Status Solidi A* 213 (1) (2016) 85–90.
- [39] W. Aigner, S. Niesar, E. Mehmedovic, M. Opel, F.E. Wagner, H. Wiggers, M. Stutzmann, Separation of semiconducting and ferromagnetic  $\text{FeSi}_2$ -nanoparticles by magnetic filtering, *J. Appl. Phys.* 114 (2013) 134308.
- [40] J.A. Donadelli, L. Carlos, A. Arques, F.S.G. Einschlag, Kinetic and mechanistic analysis of azo dyes decolorization by ZVI-assisted Fenton systems: pH-dependent shift in the contributions of reductive and oxidative transformation pathways, *Appl. Catal. B* 231 (2018) 51–61.
- [41] J.H. Ramirez, F.J. Maldonado-Hódar, A.F. Pérez-Cadenas, C. Moreno-Castilla, C.A. Costa, L.M. Madeira, Azo-dye Orange II degradation by heterogeneous Fenton-like reaction using carbon-Fe catalysts, *Appl. Catal. B* 75 (2007) 312–323.
- [42] H.P. Feng, L. Tang, J. Tang, G.M. Zeng, H.R. Dong, Y.C. Deng, L.L. Wang, Y.N. Liu, X.Y. Ren, Y.Y. Zhou, Cu-doped  $\text{Fe}@\text{Fe}_2\text{O}_3$  core–shell nanoparticle shifted oxygen reduction pathway for high-efficiency arsenic removal in smelting wastewater, *Environ. Sci. Nano* 5 (2018) 1595–1607.
- [43] L. Tang, H.P. Feng, J. Tang, G.M. Zeng, Y.C. Deng, J.J. Wang, Y.N. Liu, Y.Y. Zhou, Treatment of arsenic in acid wastewater and river sediment by  $\text{Fe}@\text{Fe}_2\text{O}_3$  nanobunches: the effect of environmental conditions and reaction mechanism, *Water Res.* 117 (2017) 175–186.
- [44] I. Sondia, V. Tomašić, N. Filipović-Vinceković, Release of silicon and aluminum from montmorillonite surfaces in aqueous systems, *Croat. Chem. Acta* 81 (4) (2008) 623–629.
- [45] T.H. Gu, J.M. Shi, Y.L. Hua, J. Liu, W. Wang, W.X. Zhang, Enrichment of silver from water using nanoscale zero-valent iron (nZVI), *Acta Chim. Sinica* 75 (2017) 991–997.
- [46] X.J. Guo, Z. Yang, H.Y. Dong, X.H. Guan, Q.D. Ren, X.F. Lv, X. Jin, Simple combination of oxidants with zero-valent-iron (ZVI) achieved very rapid and highly efficient removal of heavy metals from water, *Water Res.* 88 (2016) 671–680.